JOURNAL OF CATALYSIS **180,** 1–13 (1998)
ARTICLE NO. CA982237

Characterization of WO_x/ZrO_2 by Vibrational Spectroscopy and *n*-Pentane Isomerization Catalysis

M. Scheithauer,* T.-K. Cheung,† R. E. Jentoft,† R. K. Grasselli,* B. C. Gates,† and H. Knözinger*,[1]

*Institut für Physikalische Chemie, Universität München, Sophienstrasse 11, D-80333 Munich, Germany; and †Department of Chemical Engineering and Materials Science, University of California, Davis, California 95616

Received May 12, 1998; revised July 6, 1998; accepted July 9, 1998

Tungstated zirconia catalysts containing WO_3 loadings ranging from 3.6 to 23.9 wt% were prepared by refluxing an aqueous suspension of hydrous zirconia containing appropriate amounts of metatungstate, drying, and calcinating at 923 K or 1098 K. The acidic properties of the samples were characterized by low-temperature infrared spectroscopy with adsorbed CO as a probe molecule. Both Lewis and Brønsted acid centers with enhanced acid strength were created as the WO_3 loading increased. The Lewis sites are coordinatively unsaturated surface Zr^{4+} ions. Their density decreased significantly as the WO_3 loading approached saturation, and simultaneously the surface ZrOH groups disappeared. These observations are consistent with high (perhaps monolayer) dispersion of the surface tungstate. The Brønsted acid strength also increased with increasing WO_3 loading up to saturation and remained constant at higher loadings. These results show that large WO_3 domain or cluster sizes are required to create strong Brønsted acidity. Zr-heteropolytungstates containing charge-compensating protons are proposed as surface structures to account for the observations. The catalytic activities of these materials for *n*-pentane isomerization at 523 K in a flow reactor were found to parallel the measured Brønsted acid strengths. However, because an induction period of increasing catalytic activity was found, followed by catalyst deactivation, it is suggested that the detected Brønsted acidity may not simply account for the catalytic activity. Catalytic and *in-situ* Raman spectroscopic evidence indicates the formation of carbonaceous surface deposits during the induction period. These may be converted into catalytic sites and ultimately into deposits that cause catalyst deactivation.

INTRODUCTION

Sulfated zirconia and related catalysts have been investigated extensively because of their potential for replacing halide-type solid acids and zeolites for alkane isomerization processes (1). These nonhalide solid acids undergo rapid deactivation (2), and they may undergo sulfur loss during high-temperature reactions (3). As an alternative to sulfated zirconia, tungstated zirconia, WO_x/ZrO_2 (WZ), was also reported to be active for isomerization of C_4 to C_8 alkanes (4–7). Although WZ is much less active than sulfated zirconia, it offers an important advantage as the WO_x units in WZ are much more stable than the sulfate groups in sulfated zirconia at high temperatures (8) and in reductive atmospheres (3).

WO_x species on ZrO_2 support surfaces create strongly acidic sites (4–7,9). The WO_x species at saturation coverage on ZrO_2 inhibit ZrO_2 sintering and the tetragonal to monoclinic ZrO_2 phase transformation (6,7,9). The creation of strongly acidic centers appears to require WO_x clusters; X-ray absorption spectra (6,10) indicate that distorted octahedral W^{6+} species dominate on ZrO_2 surfaces, and UV-Vis spectra (6) demonstrate that WO_x domain sizes increase with loading. These conclusions are consistent with our own UV-Vis and Raman spectra characterizing samples having WO_3 loadings ranging from 3.6 to more than 30 wt% (9).

Apart from the information that the WO_x surface species are octahedral polymeric clusters (structurally distinct from WO_3), little is known about the structural characteristics of the WO_x overlayers. Synthesis of active catalysts requires hydrous zirconia rather than ZrO_2. We have therefore speculated (9) that Zr^{4+} might be incorporated within the polymeric clusters, forming surface analogues of molecular heteropolytungstates. This tentative structural model is consistent with our Raman and optical spectra (9). These presumed surface heteropolyoxo anions would also need protons for charge compensation, and these might be responsible for the observed Brønsted acidity. The O-H stretching bands in the infrared spectra support this suggestion (9). The acidic character of tungstated zirconias was tested by adsorption of the bases pyridine (10), 2,6-dimethylpyridine (7), and CO (at low temperature) (9), with the results all demonstrating the presence of both Lewis and Brønsted acid sites. The CO-induced red shift of the O-H stretching band of 8.6 wt% WO_3/ZrO_2[2] (a sample with saturation coverage of WO_3) was found to be

[1] Corresponding author.

[2] Loadings of WO_x are represented on the basis of the assumption that WO_x was WO_3.

0021-9517/98 $25.00

ca 160 cm^{-1} (9), almost identical to the shift observed for sulfated zirconia (11). This shift is about half that measured for the zeolite HZSM-5, which implies that tungstated zirconia is only a moderately strong solid acid; the data provide no evidence of sites with extremely strong acidity.

Catalytic tests of these solid acids (occasionally containing Pt) have been done with the isomerization of *n*-butane (10), *n*-pentane (to give 2-methylbutane) (7), and *n*-heptane (6). The catalysts typically showed high activities under mild conditions (although the required temperatures were higher than those reported for sulfated zirconias), and they had high selectivities for the isoalkanes with very little disproportionation or cracking. The *n*-pentane isomerization activity was found to pass through a maximum as the tungsten loading increased (5,7). Iglesia *et al.* (6) suggested that the reactions are bimolecular, involving hydrogen transfer from alkanes or H_2. Selective poisoning experiments with 2,6-dimethylpyridine (site titration) allowed an estimate of the density of Brønsted acid centers, revealing that only a small minority of the acid sites were very strongly acidic (7).

Here we report an investigation of the acidic character of tungstated zirconias containing between 3.6 and 23.9 wt% WO_3 by low-temperature IR spectroscopy of adsorbed CO, which permits discrimination between Lewis and Brønsted acid sites and a qualitative ranking of the acid strength based on frequency shifts of the carbonyl stretching mode of adsorbed CO and of the O-H stretching mode of acidic surface hydroxyl groups (12). The catalytic isomerization of *n*-pentane to 2-methylbutane was also investigated with the aim of correlating the acidic character of the catalysts with their activities. As in *n*-butane isomerization catalyzed by sulfated zirconias (13), there was an induction period during which the catalytic activity grew in; we also report Raman spectra characterizing hydrocarbon deposits that form on the catalyst surface (14) during the induction period and the subsequent deactivation period.

EXPERIMENTAL

Catalyst Preparation

The WZ catalysts were prepared, as described previously (9), by suspending hydrous zirconium oxide (MEL Chemicals) in aqueous solutions containing amounts of ammonium metatungstate (Fluka) sufficient to yield materials with loadings between 3.6 and 23.9 wt% WO_3 in the calcined state. The suspensions were refluxed at 383 K for 16 h, followed by evaporation of the water, drying at 383 K for 12 h, and calcination at temperatures between 773 and 1098 K for 3 h. The BET surface areas were measured with a Sorptomatic 1800 instrument (Carlo Erba) after drying of the samples at 473 K in dynamic vacuum for 1 h. The samples are listed in Table 1, together with their WO_3 loadings, surface areas, and the sample notation; the three or four digits following the sample notation indicate the calcination temperature in K.

TABLE 1

Catalyst Sample Numbers, WO_3 Contents, and BET Surface Areas of Tungstated Zirconia Samples

Catalyst sample number	WO_3 content, wt%	Calcination temperature, K	Surface area, m^2/g
Z1098	—	1098	18
3.6WZ923	3.6	923	54
3.6WZ1098	3.6	1098	30
5.9WZ923	5.9	923	64
5.9WZ1098	5.9	1098	40
8.6WZ923	8.6	923	69
8.6WZ1098	8.6	1098	46
10.5WZ923	10.5	923	82
10.5WZ1098	10.5	1098	46
13.6WZ923	13.6	923	88
13.6WZ1098	13.6	1098	42
19.0WZ773	19.0	773	119
19.0WZ923	19.0	923	96
19.0WZ1098	19.0	1098	35
23.9WZ923	23.9	923	70
23.9WZ1098	23.9	1098	30

Low-Temperature IR Spectroscopy

IR spectra were recorded with a Bruker IFS-66 FTIR spectrometer equipped with a liquid N_2-cooled MCT detector. Self-supporting wafers (ca 15–20 mg/cm^2) were pressed at ca 200 bar and pretreated in dry O_2 (50 ml (NTP)/min) at 673 K for 1 h. The pretreated samples were cooled to liquid N_2 temperature under vacuum ($<10^{-3}$ mbar) for 1.5 h. Then the spectra were measured after the samples had been exposed to CO at increasing equilibrium pressures (0.1–40 mbar).

Laser Raman Spectroscopy

The Raman spectra were recorded with the scanning multichannel technique (15) on an OMARS 89 triple-monochromator spectrometer (Dilor) equipped with a thermoelectrically cooled CCD-camera (Princeton Instruments). The 488-nm line of an Ar^+-ion laser (Spectra Physics, Type 2020) was used for excitation. A laser power of approximately 30 mW (measured at the sample position) was applied. The spectral resolution was 5 cm^{-1}. Dehydration of the samples and the subsequent catalytic isomerization reaction were carried out in a quartz flow reactor with an inner diameter of 1 cm. Before each experiment, the catalyst was heated in flowing O_2 (30 ml (NTP)/min) from room temperature to 673 K at 10 K/min, and the temperature was then held at 673 K for 1 h. After this pretreatment, the catalyst was cooled to 523 K (reaction temperature) in a 30-ml(NTP)/min flow of He for 30 min. The flow rate of

reactant, *n*-pentane (0.01 bar in carrier gas N_2), was 20 ml (NTP)/min.

n-Pentane Isomerization

Catalytic reactions were conducted in a once-through plug flow reactor at 1.01 bar (16). The reaction temperature was 523 K; the feed was a mixture of *n*-pentane and N_2, with the partial pressure of *n*-pentane being 0.01 bar. The total feed flow rate was 20 ml (NTP)/min, and the mass of catalyst was 1.0 g. Hydrocarbon products were analyzed by on-line gas chromatography (GC) with an alumina PLOT column 0.53 mm in diameter and 30 m in length and a flame-ionization detector. The first GC injection was after 5 min on stream, and 10 subsequent injections were made at intervals of 16.5 min, with subsequent injections every 60 min.

Before each reaction experiment, the catalyst was pretreated in air (30 ml (NTP)/min), heated from room temperature to 673 K at 10 K/min, and held at 673 K for 1 h. Then the catalyst was cooled to 523 K (reaction temperature) in N_2 flowing at 30 ml(NTP)/min for 30 min.

RESULTS

Low-Temperature IR Spectroscopy

O-H stretching region. Transmission IR spectra in the O-H stretching region of samples calcined at 923 K (Samples 3.6WZ923, 8.6WZ923, and 19.0WZ923) are shown in Figs. 1A–C. The high noise in the spectra is a consequence of the low transmittance of the sample wafers at frequencies greater than 3000 cm^{-1}. The background spectra (0 mbar CO) in Figs. 1A–C were recorded prior to adsorption of CO. Two bands, at 3777 and 3741 cm^{-1}, characterizing Sample 3.6WZ923 (Fig. 1A), and at 3768 and 3742 cm^{-1}, characterizing Sample 8.6WZ923 (Fig. 1B), were observed for the lower WO_3 loadings, but not in the spectrum of Sample 19.0WZ923, which had a higher WO_3 loading (Fig. 1C). All background spectra show an increased absorption at frequencies less than approximately 3700 cm^{-1}, with weak maxima near 3670 cm^{-1} for Sample 3.6WZ923 and at approximately 3630 cm^{-1} for the other two samples.

After adsorption of CO, the absorptions at 3670 and 3630 cm^{-1} were almost quantitatively eroded, even at the lowest CO equilibrium pressures, and a broad band grew in at lower wavenumbers, indicating that the CO probe underwent hydrogen bonding with OH groups. The frequency positions of the broad bands shifted relative to the weak maxima at 3670 and 3630 cm^{-1} by ca 90, 115, and 160 cm^{-1}, respectively, for the three samples as the WO_3 loading increased.

Results very similar to these were obtained for the samples calcined at 1098 K. As representative examples, Figs. 2A and B show the O-H stretching region of IR spectra of samples 3.6WZ1098 and 19.0WZ1098, respectively. Two bands (at 3772 and 3743 cm^{-1}) were observed prior to CO adsorption (Fig. 2A), but only a very weak band (at 3745 cm^{-1}) was detected in the background spectrum of Sample 19.0WZ1098 (Fig. 2B). Like the spectra of the samples calcined at 923 K, the spectrum of each of the samples calcined at 1098 K shows an increased absorption at wavenumbers less than approximately 3700 cm^{-1}, with a weak maximum between ca 3625 and 3650 cm^{-1} (Figs. 2A and B). When CO was adsorbed (Figs. 2A and B), strong broad bands developed again, with their maxima being shifted by 125 and 170 cm^{-1}, respectively, relative to the maxima in the background spectra of Samples 3.6WZ1098 and 19.0WZ1098.

The wavenumbers of the O-H stretching modes before and after CO adsorption are summarized for all the samples in Table 2, which also includes the shift of the O-H band after adsorption of CO relative to the weak maximum of the lowest-frequency O-H band.

The spectra shown in Figs. 1 and 2 and the data summarized in Table 2 demonstrate the following results:

(i) the highest-frequency O-H mode attributed to ZrOH groups eroded continuously with increasing WO_3 loading;

(ii) the intensity of this O-H mode disappeared at a loading of only 8.6 wt% WO_3 for samples calcined at 1098 K, whereas it disappeared at a loading of 13.6 wt% after calcination at 923 K;

(iii) the position of the high-frequency band of the tungstated samples at the lower loadings occurred at lower wavenumbers than that of pure zirconia and shifted to lower wavenumbers with increasing WO_3 loading (Table 2);

(iv) the shift of the O-H band induced by CO adsorption relative to the weak maximum of the low-frequency O-H mode was in all cases greater than that observed for pure zirconia and increased with increasing WO_3 loading;

(v) these frequency shifts, $\Delta\nu_{OH}$, seem to have decreased slightly with increasing CO pressure, suggesting a decrease in hydrogen bond energy with coverage;

(vi) increasing CO-induced frequency shifts, $\Delta\nu_{OH}$, were accompanied by an increasing band width, consistent with increasing hydrogen bond energy (cf. spectra in Fig. 1A and, e.g., 1C);

(vii) O-H stretching frequency shifts, $\Delta\nu_{OH}$, were larger for the samples calcined at the higher temperatures at equal loading in the range below the maximum shift. For example, the shifts were 135, 160, and 170 cm^{-1} for Samples 19.0WZ773, 19.0WZ923, and 19.0WZ1098, respectively.

CO stretching region. IR spectra in the ν_{CO} stretching region after adsorption of CO at ca 80 K are exemplified in Figs. 3A and B and Figs. 4A and B, respectively, for Samples 3.6WZ923 and 19.0WZ923 and 3.6WZ1098 and 19.0WZ1098. Three frequency regimes were typically observed, namely, 2170–2195 cm^{-1}, 2150–2160 cm^{-1}, and near 2140 cm^{-1}. The high-frequency component became saturated even at the lowest CO pressure (0.1 mbar), whereas

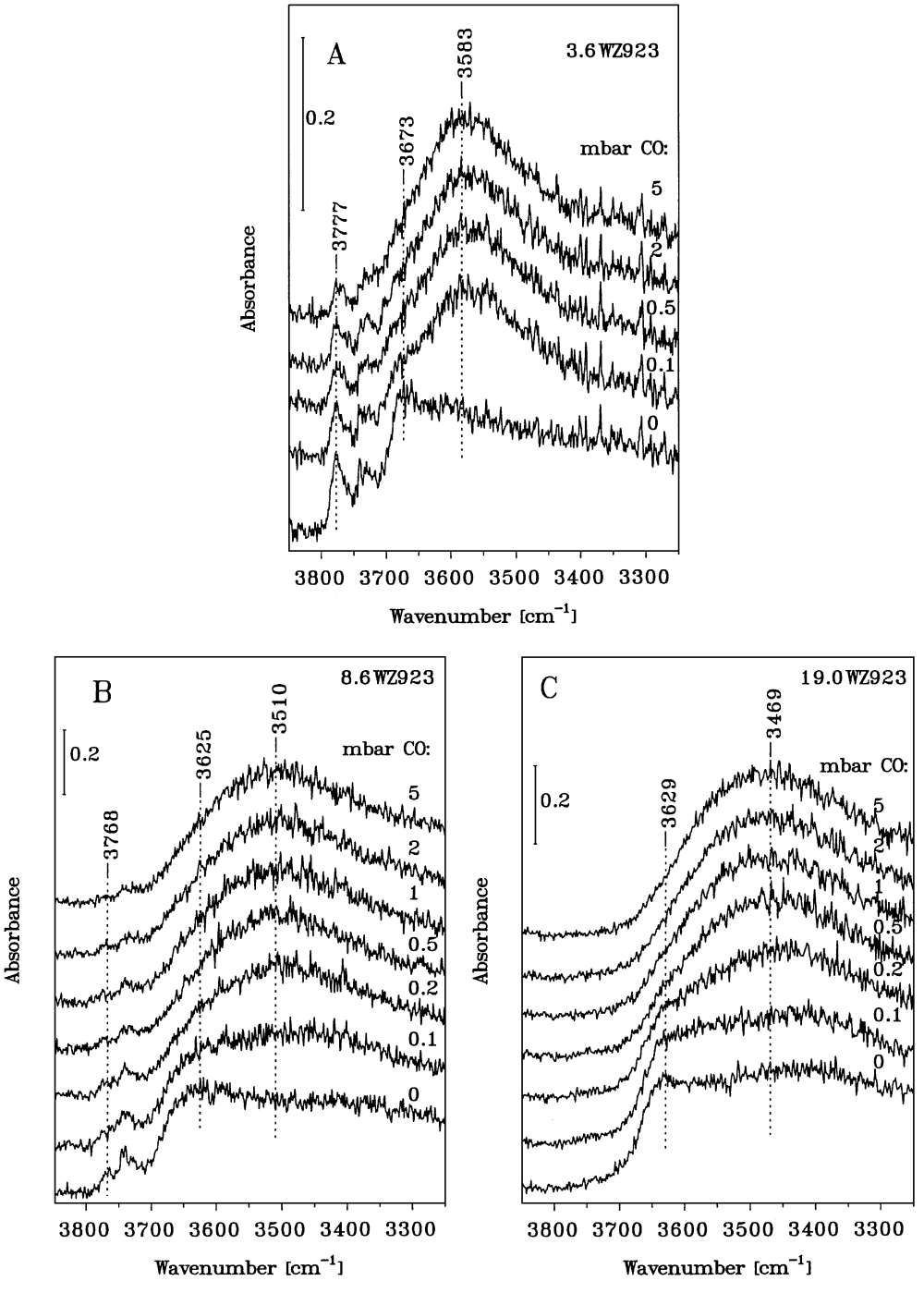

FIG. 1. Low-temperature IR spectra of the O-H stretching region of tungstated zirconia with varying WO_3 loadings calcined at 923 K prior to and after CO adsorption at ca 80 K: (A) Sample 3.6WZ923; (B) Sample 8.6WZ923; (C) Sample 19.0WZ923.

the central band required somewhat higher CO pressures for saturation. The former bands are characteristic of the strong coordination of CO molecules to cation sites (Lewis acid centers), whereas the latter bands fall into the regime characteristic of hydrogen-bonded CO (12, 17). The low-frequency component near 2140 cm^{-1} (nearly equal to the frequency of gas-phase CO, 2143 cm^{-1}), which appeared only as a shoulder and which grew in intensity with increasing CO pressure, is attributed to physisorbed CO.

These spectra clearly indicate the presence of Lewis acid centers, most likely coordinatively unsaturated Zr^{4+} centers, at WO_3 loadings well below the saturation coverage (estimated to be ca 19.0 wt% WO_3 for the samples calcined at 923 K). The band at 2176 cm^{-1} in Fig. 3A shows the

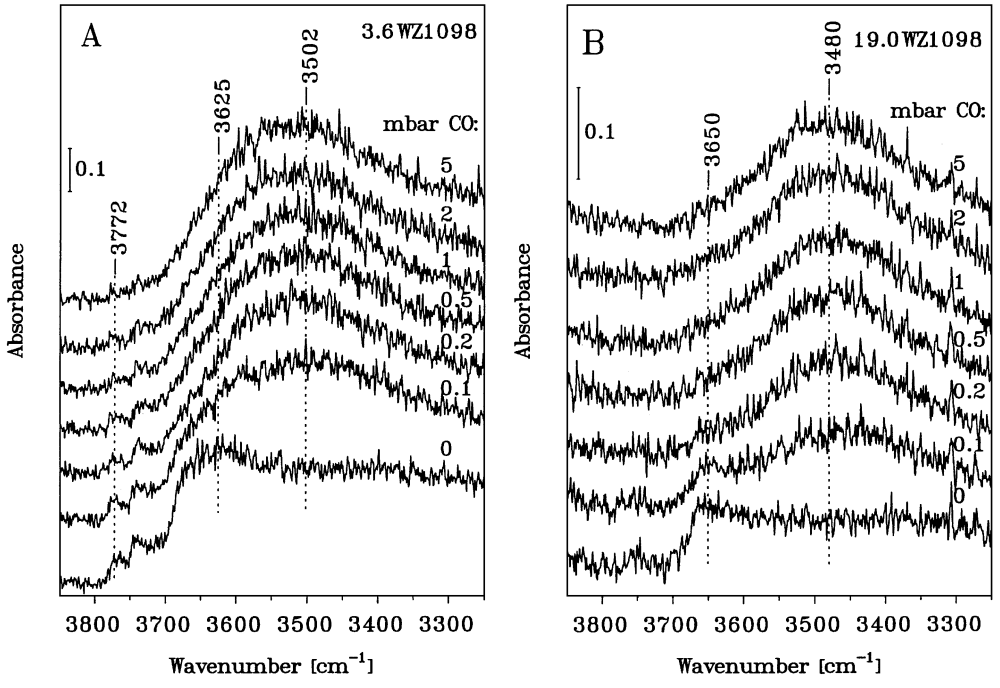

FIG. 2. Low-temperature IR spectra of the O-H stretching region of tungstated zirconia with varying WO_3 loadings calcined at 1098 K prior to and after CO adsorption at ca. 80 K: (A) Sample 3.6WZ1098; (B) Sample 19.0WZ1098.

presence of these sites on Sample 3.6WZ923. As the WO_3 loading increased, the corresponding ν_{CO} band shifted to higher frequency, ultimately becoming only a weak shoulder at 2184 cm^{-1} for Sample 19.0WZ923 (Fig. 3B). The central band of hydrogen-bonded CO, which is characteristic of Brønsted acid sites, was observed at 2157 cm^{-1} for Sample 3.6WZ923 (Fig. 3A) and at 2170 cm^{-1} for 19.0WZ923 (Fig. 3B) at low CO pressures. The band shifted to lower frequencies (closer to the gas-phase frequency) as the CO pressure increased.

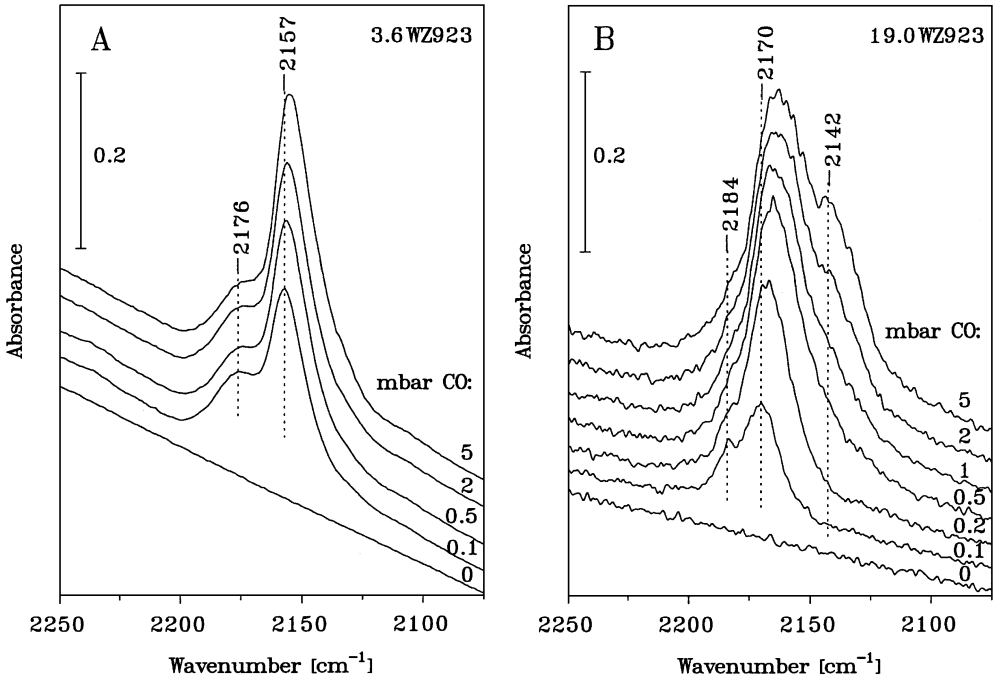

FIG. 3. Low-temperature IR spectra of CO adsorbed at ca 80 K on (A) Sample 3.6WZ923 and (B) Sample 19.0WZ923.

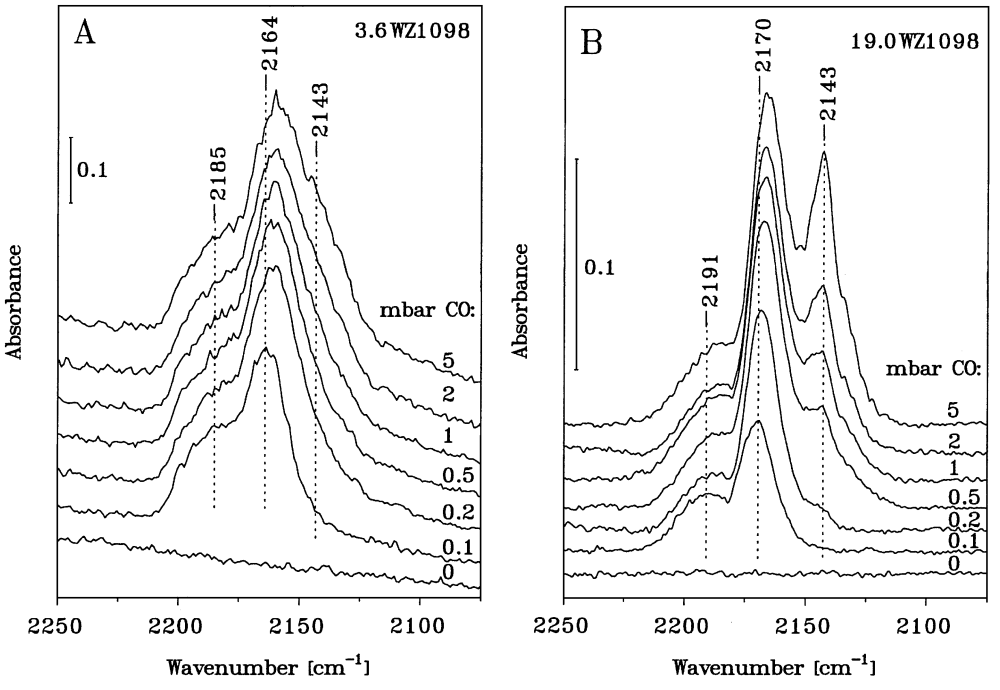

FIG. 4. Low-temperature IR spectra of CO adsorbed at ca 80 K on (A) Sample 3.6WZ1098 and (B) Sample 19.0WZ1098.

Trends similar to these are evident in the spectra of CO adsorbed on the samples calcined at 1098 K. A very broad, ill-defined absorption centered at approximately 2185 cm^{-1} was observed for the low-loaded Sample 3.6WZ1098 (Fig. 4A), whereas a far less intense band appeared at 2191 cm^{-1} in the spectrum of Sample 19.0WZ1098 (Fig. 4B). The bands of hydrogen-bonded CO are located at 2164 cm^{-1} and 2170 cm^{-1} in the spectra of Samples 3.6WZ1098 and 19.0WZ1098, respectively, at low CO pressures and shifted toward the gas-phase frequency of CO as the pressure increased.

Low-temperature adsorption of CO on all the other samples (independent of calcination temperature) gave comparable spectra. Typically, the C-O stretching frequency of the coordinated CO species increased by a few wavenumbers, whereas the intensity simultaneously decreased as the WO_3 loading approached the saturation value (10 wt% for samples calcined at 1098 K and ca 20 wt% for samples calcined at 923 K). The ν_{CO} frequency of the hydrogen-bonded CO also increased with increasing WO_3 loading and remained constant beyond saturation coverage.

W=O stretching region. Representative IR spectra in the W=O stretching region are shown in Figs. 5A–C for Samples 3.6WZ923, 8.6WZ923, and 19.0WZ923, respectively, and in Figs. 6A and B for Samples 3.6WZ1098 and 19.0WZ1098, respectively. The spectra recorded prior to adsorption of CO rather closely resemble the corresponding Raman spectra (9), although the relative intensities of the bands are different.

A broad W=O absorption band at 995 cm^{-1} is evident in the spectrum of Sample 3.6WZ923 recorded prior to adsorption of CO (Fig. 5A). This band was completely eroded after exposure to CO. The spectrum of Sample 8.6WZ923 prior to CO adsorption (Fig. 5B) shows two major broad bands (at 1017 and 1008 cm^{-1}), which shifted to 1010 and 996 cm^{-1} after exposure to CO. However, when the WO_3 loadings were high (e.g., Sample 19.0WZ923), an almost negligible shift of the W=O stretching modes at 1021 and 1014 cm^{-1} was observed after adsorption of CO (Fig. 5C), although the relative intensities and band widths changed slightly. Very similar trends were observed for the samples calcined at 1098 K (Figs. 6A and B).

The spectra in the W=O stretching region in Figs. 5A–C and 6A and B show the following results:

(i) The effect of CO on the W=O stretching modes decreased with increasing WO_3 loading;

(ii) the perturbation ceased to occur at lower WO_3 loadings for the samples calcined at the higher temperature, (e.g., for Sample 8.6WZ1098 (spectrum not shown) as compared to Sample 19.0WZ923).

n-Pentane Isomerization Catalysis

Data analysis. Normalized conversion to product containing *i* carbon atoms is defined as (moles of product formed/moles of *n*-pentane fed) × (*i*/5). The sum of the normalized conversions to products gives the *n*-pentane conversion. The selectivity to a product containing *i* carbon atoms is determined by the normalized conversion

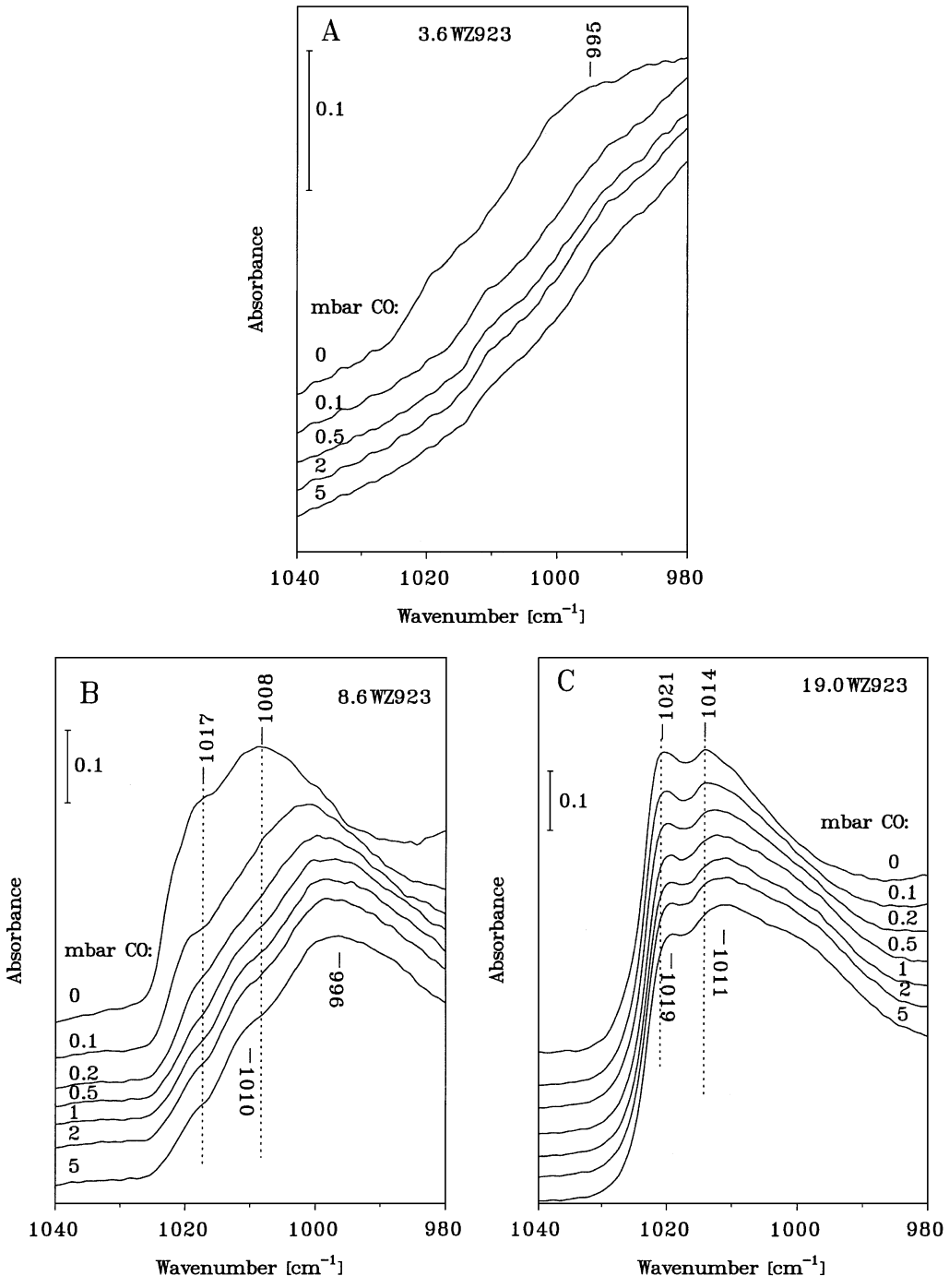

FIG. 5. Low-temperature IR spectra in the W=O stretching region prior to and after CO adsorption on (A) Sample 3.6WZ923; (B) Sample 8.6WZ923; and (C) Sample 19.0WZ923.

to the product/*n*-pentane conversion. Because the conversions were less than a few percentages, they were assumed to be differential. Thus, the rate of product formation and the rate of *n*-pentane conversion are estimated by (normalized conversion to product) × (moles of *n*-pentane fed/s × g of catalyst) and (conversion of *n*-pentane) × (moles of *n*-pentane fed/s × g of catalyst), respectively.

Performance of WZ catalysts. Several members of the two series of WZ catalysts calcined at 923 and 1098 K, respectively, were prepared twice (independently). The catalytic performances of the separate preparations at equal WO_3 loading and calcination temperature were qualitatively the same, and the rates of *n*-pentane conversion agreed within ca 20%.

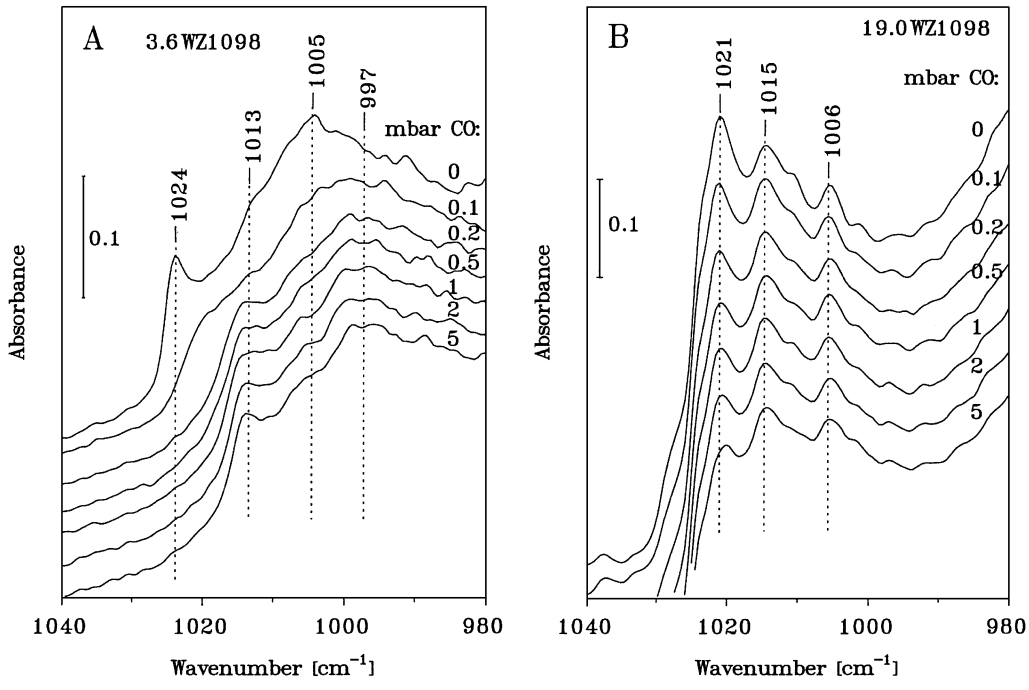

FIG. 6. Low-temperature IR spectra in the W=O stretching region prior to and after CO adsorption on (A) Sample 3.6WZ1098; and (B) Sample 19.0WZ1098.

Not all the WZ samples were active for conversion of *n*-pentane at 523 K and a *n*-pentane partial pressure of 0.01 bar. For example, the samples with WO_3 loadings of 3.6 wt% and 5.9 wt% calcined at 1098 K and the samples with WO_3 loadings of 8.6 and 10.5 wt% calcined at 923 K gave negligible or extremely low conversions, suggesting that only larger oxide clusters or patches provide catalytically active structures. In the presence of the active WZ catalysts, the observed products of *n*-pentane conversion were isopentane, isobutane, propane, and traces of hexanes and *n*-butane. The products indicate the occurrence of isomerization accompanied by disproportionation and cracking, consistent with acid–base catalysis. The colors of the active catalysts changed from white or slightly yellow to gray after operation.

Figure 7 shows a typical dependence of the rate of *n*-pentane conversion on time-on-stream (TOS) for catalyst Sample 19.0WZ923. The rate at zero TOS was essentially zero, increasing with TOS and passing through a maximum. All of the active catalysts showed this qualitative behavior. We refer to the period prior to the maximum as the induction period and that following as the deactivation period. The time to the maximum rate was less for catalysts exhibiting higher activities. The rate of deactivation was lower for catalysts having lower activities. The selectivities to 2-methylbutane (isopentane) were between 60 and 80%, being only slightly dependent on TOS. Typically, the most active catalysts (e.g., Sample 19.0WZ923) also showed the highest isomerization selectivity.

As a basis for a comparison of the activities of catalysts with different WO_3 loadings, the maximum rates of *n*-pentane conversion measured at 523 K as a function of TOS were chosen; this choice is arbitrary but conventional for sulfated and tungstated ZrO_2. This maximum rate is shown in Figs. 8A and B as a function of WO_3 loading and calcination temperature. The activities of samples containing less than approximately 8 wt% WO_3 were almost negligible, independent of the calcination temperature. The catalysts calcined at 1098 K are characterized by activities that rise relatively steeply with increasing WO_3 content,

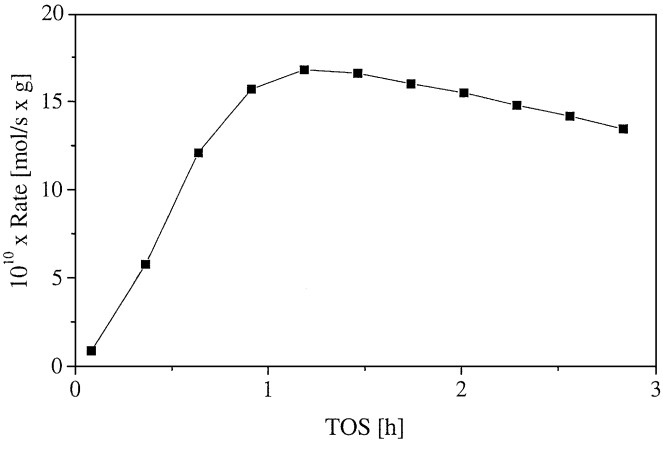

FIG. 7. Rate of *n*-pentane conversion as function of time on stream in a flow reactor at 523 K.

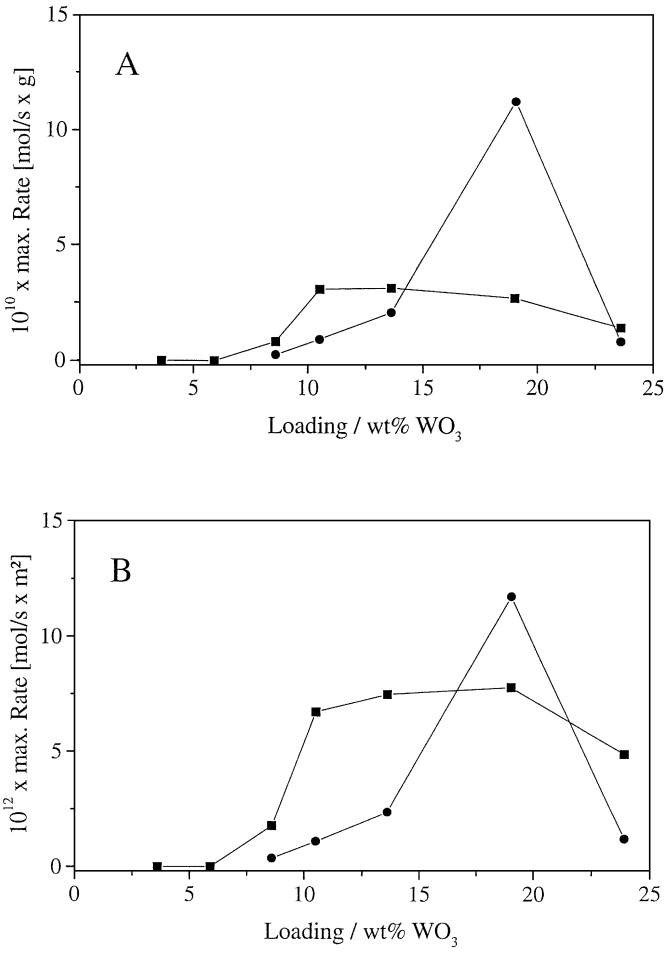

FIG. 8. Dependence of rate of *n*-pentane conversion at the end of the induction period on WO_3 loading at 523 K: A, rate per unit mass; B, rate per unit surface area; -■- Sample xWZ1098; -●- Sample xWZ923.

reaching a plateau near 10 wt% WO_3, and declining beyond 20 wt% WO_3. The rise in rates below ca 15 wt% WO_3 was less pronounced for the catalysts calcined at 923 K than for the others. At 19 wt% WO_3 a relatively sharp maximum was observed (the highest rate measured), followed by a steep decline beyond ca 20 wt% WO_3.

Several experiments with interrupted *n*-pentane flow were conducted in attempts to shed light on the phenomena occurring during the induction period. The most active catalyst, Sample 19.0WZ923, was chosen for these experiments, and the results are shown in Fig. 9. The experimental conditions were the same as those used in the experiment represented by the data of Fig. 8, and the dotted curve in Fig. 9 corresponds to the rate versus the TOS plot of Fig. 8A. A comparison of the dotted line and curve b in Fig. 9 shows the excellent reproducibility of rates of *n*-pentane conversion within the induction period. The reactant feed flow was interrupted at 40 min TOS (arrow in Fig. 9), at which time the color of the catalyst had changed from white to light gray; then the reactor was purged with dry N_2 (50 ml(NTP)/min) at 523 K for 45 min. The reactant flow was then restarted, and the rate determined as a function of the TOS, with time zero being the time when flow was restarted (curve c, Fig. 9). The initial rate was now nonzero, increasing with TOS and appearing to reach a flat maximum at a lower rate than that shown by curve a for the uninterrupted operation. The reactant flow was again interrupted after 75 min into the second operating period. An N_2 purge followed, as described above, and the reactant flow was started a third time (curve d, Fig. 9). The initial rate now had a still higher value, increasing only slightly with the TOS to a plateau at a lower rate than the maxima of curves a and c; a slow decline in rate followed. The reaction was interrupted again at 90 min into the third period, and the catalyst was regenerated in flowing air (30 ml(NTP)/min) at 673 K for 1 h and then purged with dry N_2 (30 ml(NTP)/min) at 523 K for 30 min. The rate of *n*-pentane conversion was then measured again as a function of the TOS, with the data represented by curve e in Fig. 9. This curve qualitatively reflects the behavior of the fresh catalyst, but the original activity was not regained after the regeneration.

The results of these experiments are consistent with the suggestion that some hydrocarbon deposits formed during the course of the reaction; these might be responsible for both the induction period and the deactivation. An attempt was made to elucidate the nature of these deposits by *in-situ* Raman spectroscopy within the time frame of the induction period.

Laser Raman Spectroscopy

The Raman spectra shown in Fig. 10 were recorded at 523 K with the most active catalyst, Sample 19.0WZ923, in

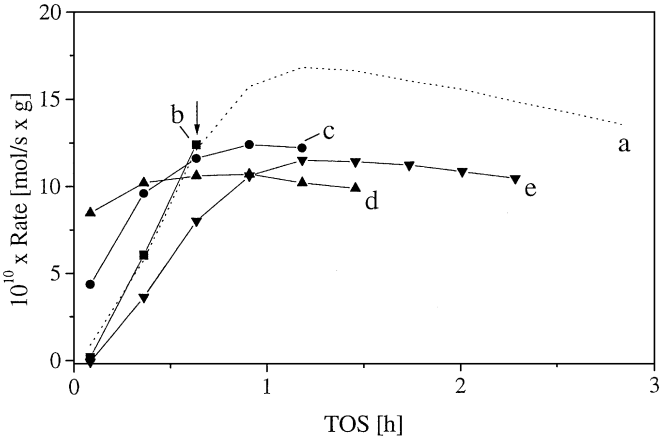

FIG. 9. Dependence of rate of *n*-pentane conversion on time on stream in a flow reactor at 523 K: (a) same as Fig. 8; (b) fresh sample; (c) after interruption of (b) at 40 min and purging with N_2 at 523 K for 45 min; (d) after interruption of (c) at 75 min and purging with N_2 at 523 K for 45 min; (e) after regeneration in flowing air at 673 K for 1 h and purging with N_2 at 523 K for 30 min.

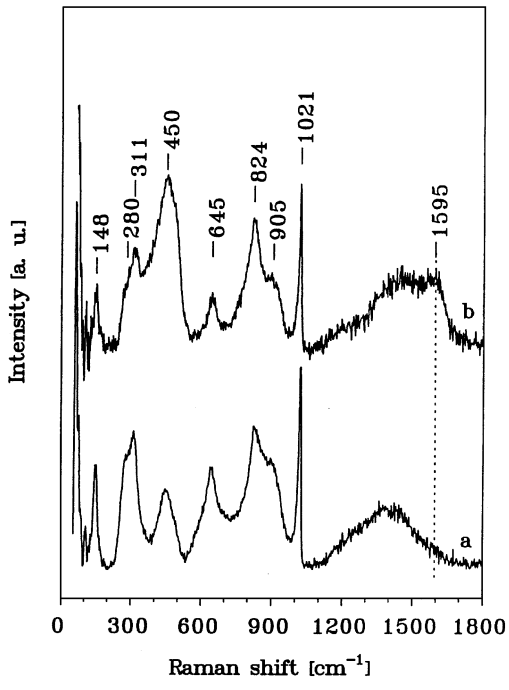

FIG. 10. *In-situ* Raman spectra of Sample 19.0WZ923 at 523 K in flowing He (a) after pretreatment at 673 K for 1 h in flowing O_2 and subsequent cooling to 523 K in flowing He for 30 min and (b) after 15 min reaction of *n*-pentane (0.01 bar in N_2) and subsequent purging with dry He for 5 min. Spectra are baseline corrected.

flowing He. The experimental conditions were comparable to those used in the catalytic experiments represented by the data of Fig. 9. The catalyst was pretreated in a quartz flow reactor at 673 K for 1 h in flowing O_2. After subsequent cooling to 523 K (the reaction temperature) in flowing He for 30 min, a spectrum of the pretreated sample prior to reaction was recorded. Figure 10a shows the bands of tetragonal ZrO_2 (bands at 148, 280 (sh), 311, 452, and 645 cm^{-1}) and the typical feature of the WO_x overlayer in the high-frequency region between ca 824 and 1021 cm^{-1} (9). The broad band near 1400 cm^{-1} is an artifact.

The catalytic reaction was started with a flow of *n*-pentane (0.01 bar in N_2) of 20 ml(NTP)/min. After 15 min on stream, the reactant feed was interrupted and the reactor purged with dry He (30 ml(NPT)/min) for 5 min before the Raman spectrum of Fig. 10b was recorded. The data indicate no significant change in the high-frequency region between ca 824 and 1021 cm^{-1} characterizing the WO_x overlayer; the bands of the ZrO_2 support were still observed. However, new bands at ca 1595 and 450 cm^{-1} and weak bands near 3000 cm^{-1} (the latter not shown) were detected (Fig. 10b). These results support the suggestion of the formation of hydrocarbon deposits within the induction period, which are hypothesized to play a role in the genesis of the catalytic sites. Raman spectra were also recorded after 30, 45, and 105 min on stream. The intensities of the bands at 445 and near 1595 cm^{-1} increased and after 105 min a new shoulder near 1206 cm^{-1} could be observed. Although catalytic activity is highest after 105 min on stream (Fig. 9), the formation of coke has most probably started at this point.

DISCUSSION

Structural Considerations

The formation of tungsten oxide clusters on ZrO_2 has been suggested (6,9), with the spectroscopic evidence showing that the cluster dimensions grow with increasing WO_3 loading. These clusters are presumably anchored to the ZrO_2 surface via Zr-O-W linkages, and WO_3 microcrystallites presumably become detectable only at loadings beyond the saturation coverage (9). Estimated saturation coverages are ca 20 wt% WO_3 for the series of samples calcined at 923 K (BET surface area, $S_{BET} = 96$ m^2/g) and ca 10 wt% WO_3 for those calcined at 1098 K ($S_{BET} = 46$ m^2/g). A tentative structural model is based on the assumption of the formation of Zr-heteropolytungstate-type species containing charge-compensating protons (9). These protons might be delocalized within the tungstate species and might be located in hydrogen-bonded units by sharing several oxo groups, as has been shown (18,19) for molecular tungsten polyoxo anions. We have proposed (9) that such structural units would explain the very broad, almost continuous absorption in the O-H stretching absorption region of dehydrated Sample 19.0WZ923, which ranges from around 3650 cm^{-1} to less than 3000 cm^{-1} even prior to adsorption of any probe molecules. These same broad absorptions have now been observed for the present series of samples over the entire loading range (Figs. 1A–C). The absorbance appears to be greater and to maintain higher values at low frequencies for samples with higher loadings. Relatively broad bands are evident at the high-frequency edge of the continuous absorption, near 3670 cm^{-1} for the sample with a low loading (3.6WZ923) and between 3620 and 3630 cm^{-1} for the samples with higher loadings (8.6WZ923 and 19.0WZ923). Analogous features were also observed for the samples calcined at 1098 K (Figs. 2A and B).

Furthermore, sharper O-H stretching bands were detected between 3760 and 3780 cm^{-1} at low WO_3 loadings (Figs. 1A and B and 2A). These bands are almost certainly caused by residual Zr-OH groups. Pure zirconia shows bands for terminal and bridging OH groups at 3780 and 3680 cm^{-1}, respectively (20a,20b). The positions of the residual bands in the spectra of the tungstated samples, which vary slightly with WO_3 loading, are presumably affected by indirect interactions with surface WO_x species.

The intensities of these bands were found to decrease with increasing WO_3 loading and to disappear near saturation coverage (Figs. 1A–C and 2A, B). For example, no bands of isolated Zr-OH groups were detected for Sample 19.0WZ923 (Fig. 1C), the loading of which corresponds to the estimated saturation value. It appears that during the

nucleation and growth of ZrO_2 in the presence of tungstates starting from hydrous zirconia, the surface crystallite planes are preferentially terminated by formation of Zr-O-W linkages rather than OH groups. This interpretation is consistent with the proposed monolayer formation via anchored polytungstate-like species.

These conclusions are further supported by the infrared spectra of CO adsorbed on coordinatively unsaturated cation sites. The carbonyl bands appearing between 2170 and 2190 cm^{-1} at loadings below saturation coverage (Fig. 3A and 4A) can be attributed to $Zr^{4+} \leftarrow CO$ complexes (21). There is no evidence for the formation of $W^{6+} \leftarrow CO$ complexes, the carbonyl stretching frequencies of which are known to be located at 2200 cm^{-1} (22). As the WO_3 loading increased in the series of samples calcined at 923 K, the intensity of the carbonyl bands of $Zr^{4+} \leftarrow CO$ complexes continuously decreased, with the bands disappearing near saturation coverage (Fig. 3B). Hence we conclude that coordinatively unsaturated Zr^{4+} sites are no longer accessible when saturation coverage is reached and a monolayer of polyoxo species has formed.

The situation seems to be somewhat more complex for the samples calcined at 1098 K, as a band at 2191 cm^{-1} was still detectable even when the WO_3 loading was highest (although at relatively low intensity relative to that of the band at 2170 cm^{-1}, indicative of hydrogen-bonded CO, Fig. 4B). This result may be explained by some structural and morphological changes occurring during the high-temperature calcination, during which considerable sintering takes place, as indicated by the surface area decrease (Table 1); thus, the saturation loading of the ZrO_2 support was exceeded and WO_3 microcrystallites formed (9).

The high-frequency shift of the carbonyl band of coordinated CO observed as the loading increased suggests that the coordinatively unsaturated Zr^{4+} centers interact with nearby polytungstate species via inductive effects. Conversely, coordination of CO on Zr^{4+} affects the vibrational characteristics of neighboring polytungstate species, namely the W=O stretching mode, as shown in Figs. 5A–C and 6A and B. It is clear from the spectra that this effect was observed only at coverages below saturation, when $Zr^{4+} \leftarrow CO$ complexes are formed. Hence, these results are also consistent with those stated above and support the monolayer model for the tungstated zirconia catalysts.

Acidic Properties of WZ Catalysts

An implication of the results discussed in the previous section is that the coordination of CO to Zr^{4+} at WO_3 loadings below saturation indicates the presence of Lewis acid centers. The acid strength of these centers is enhanced by the presence of surface polytungstate species, as indicated by the blue shift of the carbonyl stretching band with increasing loading. Simultaneously, the density of these sites is reduced by the increasing coverage of the ZrO_2 surface. The detection of enhanced Lewis acidity is consistent with literature reports (7,10).

The presence of Brønsted acidity is also clearly demonstrated by the low-temperature CO adsorption experiments (Figs. 1A–C and 2A and B). Typically, adsorption of CO erodes the bands or shoulders occurring at 3670 and around 3620–3630 cm^{-1}, and new broad bands grow in lower frequencies. The red shift of these bands, the increased integral intensity, and the large width is unequivocal evidence of the formation of hydrogen bonds between OH groups and the weak base CO (23). Simultaneously, bands grow in the carbonyl stretching region (Figs. 3A and B and 4A and B) between 2157 and 2170 cm^{-1}, which are characteristic of hydrogen-bonded CO (12).

The red shift of the O-H stretching mode with respect to the high-frequency component of the broad background absorption is clearly dependent on the WO_3 loading and—for a given loading—on the calcination temperature, as shown by the summary of data in Table 2. The carbonyl stretching frequency also depends on WO_3 loading and consistently shifts to higher values as the O-H stretching frequency shift ($\Delta\nu_{OH}$) increases; this result is indicative of increasing hydrogen-bond donor strength and, hence, Brønsted acid strength. As the CO pressure increased, $\Delta\nu_{OH}$ values decreased slightly, and the corresponding C-O stretch shifted to a lower frequency. This result suggests that CO interacts with weaker sites as the coverage increases, consistent with a distribution of strengths of acidic sites.

The $\Delta\nu_{OH}$ values of WZ materials range from between approximately 90 to 170 cm^{-1} and are thus significantly larger than the shift of 60 cm^{-1} observed for pure ZrO_2 (Table 2). The presence of polytungstate species therefore undoubtedly induces enhanced Brønsted acidity. The

TABLE 2

$\tilde{\nu}_{OH}$ Prior to and after Adsorption of CO at ca 80 K and $\Delta\tilde{\nu}_{OH}$

Sample	$\tilde{\nu}_{OH}$[cm^{-1}] without CO		$\tilde{\nu}_{OH}$[cm^{-1}] with 40 mbar CO		$\Delta\tilde{\nu}_{OH}$ [cm^{-1}]
Z1098	3782	~3682	3777	~3621	~60
3.6WZ1098	3772	~3625		~3502	~125
5.9WZ1098	3772	~3625		~3464	~160
8.6WZ1098		~3625		~3464	~160
10.5WZ1098		~3640		~3472	~170
13.6WZ1098		~3625		~3456	~170
19.0WZ1098		~3650		~3480	~170
23.9WZ1098		~3628		~3460	~170
3.6WZ923	3777	~3673	3773	~3583	~90
5.9WZ923	3775	~3625	3768	~3526	~100
8.6WZ923	3768	~3625		~3510	~115
10.5WZ923	3768	~3625		~3500	~125
13.6WZ923		~3634		~3510	~125
19.0WZ923		~3629		~3469	~160
23.9WZ923		~3627		~3465	~160
19.0WZ773	3765	~3658	3765	~3522	~135

highest $\Delta\nu_{OH}$ values, however, are still significantly lower than those reported for HZSM-5 (24,25). Consistent with earlier results (9), these data show that tungstated zirconia catalysts can be classified as moderately strong solid acids; the data give no evidence of extremely strong acidic sites.

It is not clear what role the delocalized protons in the polyoxo anions play, if any. They may contribute to the hydrogen-bonding interaction with CO (and become localized), or they may remain inaccessible to CO.

Clearly, the $\Delta\nu_{OH}$ values in Table 2, which are a measure of the Brønsted acid strength, increased as the WO_3 loading increased and approaching a maximum value of ca 170 cm^{-1} for the samples calcined at 1098 K and a value of ca 160 cm^{-1} for the samples calcined at 923 K as the saturation coverage was reached. The formation of WO_3 microcrystallites inferred to occur at loadings beyond saturation apparently does not influence the Brønsted acid strength. The evolution of the $\Delta\nu_{OH}$ values with loading parallels the growth of oxide domains (6,9) and therefore suggests that large domains are required to create the higher acid strength. We infer that this trend is consistent with the presence of heteropolytungstate species containing charge-compensating protons.

Catalytic Properties of WZ

As shown in Fig. 8, the rates at the end of the induction period measured as a function of the TOS increased from very low values at low WO_3 loadings to a maximum at 19.0 wt% WO_3 for the catalysts calcined at 923 K; the rate decreased at higher loadings. The maximum rate was reached at 10 wt% WO_3 for the catalysts calcined at 1098 K and declined only gradually at higher loadings. In both series of samples, the maximum rates were attained near the corresponding saturation loadings. The observed trends closely resemble those observed for the Brønsted acid strength as measured by the CO-induced O-H stretching frequency shifts (Table 2). We caution, however, that this correlation should not be overinterpreted: First, the argument only takes the acid strength into account and neglects any variation in site densities. Second, the rates were not recorded under steady-state conditions but were somewhat arbitrarily chosen as the maximum rates observed as a function of TOS. But it is tempting to suggest that the correlation is significant, in part because Santiesteban *et al.* (7) reported a similar dependence of *n*-pentane isomerization rate on WO_3 loading for catalysts prepared by coprecipitation. Santiesteban's rates were measured under nearly steady-state conditions, as the reaction was carried out in the presence of H_2 at elevated pressure, which stabilizes the catalyst.

We suggest that the activities of these materials are not controlled simply by the measured Brønsted acid strengths. Evidence consistent with this suggestion includes the following: The decline in activity at WO_3 loadings beyond saturation is not accompanied by a decrease in acid strength (Table 2). The formation of microcrystalline WO_3 may lead to surface blocking. Furthermore, phosphated zirconia gave approximately the same CO-induced O-H stretching frequency shifts (26) as the most active tungstated zirconia, but they were inactive for *n*-pentane isomerization, even at 673 K (27). The suggestion of Santiesteban *et al.* (7) that only a minority of strong acid sites would be responsible for the catalytic conversion of *n*-pentane is not completely excluded. Such a suggestion has been made for sulfated zirconia catalysts, and there is evidence that a minority of sites on this catalyst could even be strong enough to initiate reaction by protonating alkanes (28). In the present case, however, the initial activity of fresh catalysts is zero at zero time-on-stream. This result appears to be inconsistent with the assumption of a small fraction of very strong acid sites which would lead to a finite activity at zero time-on-stream.

In this context we have attempted to estimate the number of acid sites from the intensities of carbonyl stretching bands. Unfortunately the extinction coefficients of H-bonded CO molecules are not known very accurately and they are, moreover, dependent on the carbonyl stretching frequency (29). For this reason, estimates of site densities are not accurate enough to make any reliable comparisons of Brønsted acid site densities for different catalysts.

Most interesting in this context is the occurrence of an induction period. Numerous investigators observed similar behavior for the *n*-butane isomerization (e.g., 13,16) and *n*-pentane isomerization (30) on sulfated zirconias, and Alvarez *et al.* (13) argued that the formation of carbonaceous deposits has a direct relationship with the low-temperature activity. The experiments with interrupted reaction (Fig. 9) are similarly suggestive of the influence of deposits on the catalytic performance. The results also indicate that the processes occurring during the induction period and the formation of deposits, which ultimately leads to deactivation, are not independent of each other.

n-butane isomerization on sulfated zirconia involves a bimolecular mechanism, as shown by the use of doubly ^{13}C-labelled *n*-butane as a reactant by Adeeva *et al.* (31). This mechanism, which avoids the formation of primary carbenium ions, was first proposed by Guisnet (32) for the *n*-butane isomerization catalyzed by H-mordenite. Similarly, a bimolecular mechanism, has been inferred for *n*-pentane isomerization catalyzed by promoted sulfated zirconia (30). It has been speculated (14) that the C_8^+ carbocations initially formed from *n*-butane may undergo side reactions to form polyenylic and cyclopentadienyl cations, which can be considered to be precursors of aromatic coke (33). The presence of polyenylic and aromatic compounds has been demonstrated on deactivated sulfated zirconia by *in-situ* Raman and UV-Vis spectroscopy (14,34). Although the Raman spectra recorded during the induction period of *n*-pentane conversion on Sample 19.0WZ923 (Fig. 10) cannot be fully interpreted yet, the band that appears

between 1580 and 1600 cm^{-1} can undoubtedly be attributed to alkenic and/or aromatic species (14,34,35). Taking this and the previously cited results for sulfated zirconias into account, we speculate that formation of perhaps dimeric carbocations may be initiated by some minority sites on the fresh catalyst surface. These carbocations may then start chain reactions and create catalytic sites that involve the carbonaceous deposits. These and the initially formed carbocations may, however, also undergo side reactions that ultimately lead to coke formation and catalyst deactivation. These suggestions account, at least qualitatively, for the dependence of *n*-pentane conversion on TOS.

CONCLUSIONS

Tungstated zirconia catalysts develop enhanced Lewis and Brønsted acidity as the WO_3 loading is increased. The densities of cus Zr^{4+} Lewis sites decrease significantly as the loading approaches saturation and the density of original ZrOH groups declines. These changes are consistent with formation of a monolayer consisting presumably of polyoxo compounds of tungsten. The Brønsted acid strength increases with increasing WO_3 loading up to saturation, suggesting that formation of large oxide clusters results in the creation of Brønsted acidity. A tentative structure is proposed which involves surface analogues of Zr-heteropolytungstates anchored to the surface via Zr-O-W linkages. These surface species are also supposed to incorporate protons as charge-compensating cations.

The catalytic activity for *n*-pentane isomerization seems to parallel the Brønsted acid strength measured by the IR spectra of adsorbed CO. However, doubts remain as to whether the detected Brønsted acidity is responsible for the catalytic activity, since the reaction rate at zero time-on-stream is essentially zero. An induction period was observed during the catalysis followed by deactivation. It is suggested that carbonaceous deposits are initially formed—perhaps carbocations—which may be converted into catalytic sites. The carbonaceous deposits may undergo reactions leading ultimately to coke formation and catalyst deactivation.

ACKNOWLEDGMENTS

The work done in Munich was supported financially by the Deutsche Forschungsgemeinschaft (SFB 338), the Bayerische Forschungsverbund Katalyse FORKAT, and the Fonds der Chemischen Industrie. The cooperation with the University of California, Davis, USA, was made possible by generous support by the Alexander von Humboldt–Stiftung, the Max Planck–Gesellschaft, and the BMBF (Max Planck-Research Award to H.K.). The work done in Davis was supported by the University of California Energy Institute.

REFERENCES

1. Yamaguchi, T., *Appl. Catal.* **6**, 1 (1990).
2. Yori, J. C., Luy, J. C., and Parera, J. M., *Catal. Today* **5**, 493 (1989).
3. Ng, F. T. T., and Horvát, N., *Appl. Catal. A* **123**, L195 (1995).
4. Hino, M., and Arata, K., *J. Chem. Soc. Chem. Commun.*, 1259 (1988).
5. Arata, K., and Hino, M., *in* "Proc. 9th Int. Congr. Catal., Calgary, 1988" (M. J. Phillips and M. Ternan, Eds.), p. 1727. Chem. Inst. of Canada, Ottawa, 1988.
6. Iglesia, E., Barton, D. G., Soled, S. L., Moseo, S., Baumgartner, J. E., Gates, W. E., Fuentes, G. A., and Meitzner, G. D., *in* "Proc. 11th Int. Congr. Catal., Baltimore 1996," *Stud. Surf. Sci. Catal.* **101**, 533 (1996).
7. Santiesteban, J. G., Vartuli, J. C., Han, S., Bastian, D., and Chang, C. D., *J. Catal.* **168**, 431 (1997).
8. Larsen, G., Lotero, E., Parra, R. D., Petkovic, L. M., Silva, H. S., Raghavan, S., *Appl. Catal. A* **130**, 213 (1995).
9. Scheithauer, M., Grasselli, R. K., and Knözinger, H., *Langmuir* **14**, 3019 (1998).
10. Larsen, G., Lotero, E., and Parra, R. D., *in* "Proc. 11th Int. Congr. Catal., Baltimore 1996," *Stud. Surf. Sci. Catal.* **101**, 543 (1996).
11. Spielbauer, D., Mekhemer, G. A. H., Zaki, M. I., and Knözinger, H., *Catal. Lett.* **40**, 71 (1996).
12. Knözinger, H., *in* "Handbook of Heterogeneous Catalysis" (G. Ertl, H. Knözinger, and J. Weitkamp, Eds.), Vol. 2, p. 707. Wiley-VCH, Weinheim, 1997.
13. Alvarez, W. E., Liu, H., and Resasco, D. E., *Appl. Catal. A: General* **162**, 103 (1997).
14. Knözinger, H., *Top. Catal.* **6**, 107 (1998).
15. Knoll, P., Singer, R., and Kiefer, W., *Appl. Spectrosc.* **44**, 776 (1990).
16. Cheung, T.-K., d'Itri, J. L., and Gates, B. C., *J. Catal.* **151**, 464 (1995).
17. Zaki, M. I., and Knözinger, H., *J. Catal.* **119**, 311 (1989).
18. Kozhevnikov, I. V., Sinema, A., Jansen, R. J. J., and van Bekkum, H., *Mendeleev, Commun.* **92** (1994). [*Catal. Lett.* **27**, 187 (1994)]
19. Kozhevnikov, I. V., Sinnema, A., and van Bekkum, H., *Catal. Lett.* **34**, 213 (1995).
20a. Tretyakov, N., Pozdnyakov, E., Ornaskaya, O. M., and Filimonov, V. N., *Russ. J. Phys. Chem.* **44**, 596 (1970).
20b. Agron, P. A., Fuller, E. L., Jr., and Holmes, H. F., *J. Colloid Interf. Sci.* **52**, 553 (1975).
21. Zaki, M. I., Vielhaber, B., and Knözinger, H., *J. Phys. Chem.* **90**, 3176 (1986).
22. Hilbrig, F., Schmelz, H., and Knözinger, H., *in* "Proc. 10th Int. Congr. Catal., Budapest, 1992" (L. Guczi, F. Solymori, and P. Tétényi, Eds.), p. 1351. Akad. Kiado, Budapest, 1993.
23. Pimentel, G. C., and McClellan, A. L., "The Hydrogen Bond," Freeman, San Francisco/London, 1960.
24. Kustov, L. M., Kazansky, V. B., Béran, S., Kubelkova, L., and Jiru, P., *J. Phys. Chem.* **91**, 5247 (1987).
25. Mirsojew, I., Ernst, S., Weitkamp, J., and Knözinger, H., *Catal. Lett.* **24**, 235 (1994).
26. Spielbauer, D., Mekhemer, G. A. H., Riemer, T., Zaki, M. I., and Knözinger, H., *J. Phys. Chem. B* **101**, 4681 (1997).
27. Nakaoka, C., and Knözinger, H., unpublished results.
28. Cheung, T.-K., and Gates, B. C., *Top. Catal.* **6**, 41 (1998).
29. Brown, T. L., and Darensbourg, D. J., *Inorg. Chem.* **6**, 971 (1967).
30. Rezgui, S., and Gates, B. C., *Catal. Lett.* **37**, 5 (1996).
31. Adeeva, V., Lei, G. D., and Sachtler, W. M. H., *Appl. Catal. A: General* **118**, L11 (1994).
32. Guisnet, M., *Acc. Chem. Res.* **23**, 392 (1990).
33. Sommer, J., Sassi, A., Hachoumy, M., Jost, R., Karlsson, A., and Ahlberg, P., *J. Catal.* **171**, 391 (1997).
34. Spielbauer, D., Mekhemer, G. A. H., Bosch, E., and Knözinger, H., *Catal. Lett.* **36**, 59 (1996).
35. Guisnet, M., *in* "Handbook of Heterogeneous Catalysis" (G. Ertl, H. Knözinger, and J. Weitkamp, Eds.), Vol. 2, p. 626. Wiley-VCH, Weinheim, 1997.